

## RESEARCH LETTER

10.1002/2017GL072510

## Key Points:

- CMIP5 simulations show large intermodel variability in surface albedo during boreal summer
- Albedo variability is coherent on global scales and correlates with tropical rainfall variability
- Evidence supports the hypothesis that intermodel albedo variability causes intermodel rainfall variability in CMIP5 simulations

## Supporting Information:

- Supporting Information S1

## Correspondence to:

X. J. Levine,  
xavier.levine@yale.edu

## Citation:

Levine, X. J., and W. R. Boos (2017), Land surface albedo bias in climate models and its association with tropical rainfall, *Geophys. Res. Lett.*, *44*, doi:10.1002/2017GL072510.

Received 8 JAN 2017

Accepted 5 JUN 2017

Accepted article online 8 JUN 2017

## Land surface albedo bias in climate models and its association with tropical rainfall

Xavier J. Levine<sup>1</sup>  and William R. Boos<sup>1</sup> <sup>1</sup>Department of Geology and Geophysics, Yale University, New Haven, Connecticut, USA

**Abstract** The influence of surface albedo on tropical precipitation is widely appreciated, but albedo bias over snow-free areas in climate models has been studied little. Here historical Coupled Model Intercomparison Project Phase 5 simulations are shown to exhibit large multimodel mean bias and intermodel variability in boreal summer mean surface broadband shortwave albedo. Intermodel variability in this albedo is globally coherent over vegetated regions and correlates with intermodel tropical precipitation variability. Evidence supports the hypothesis that these spatially coherent albedo variations cause precipitation variations. Specifically, spatial structures of albedo and precipitation variations are distinct, suggesting the latter do not cause the former by darkening soil. Furthermore, simulated interannual albedo variance is small compared to intermodel albedo variance, while the ratio of interannual to intermodel precipitation variance is much larger. Finally, imposing the dominant pattern of intermodel albedo variability in one climate model causes a precipitation change with structure similar to that of the intermodel variability.

### 1. Introduction

Since the seminal work of *Charney* [1975], surface albedo has been recognized as a major influence on climate over a wide range of time scales, from subseasonal to orbital. On centennial time scales, surface albedo changes in boreal regions may have helped foster global glaciation, as forests changed to grasslands during the initial cooling of glacial onset [*de Noblet et al.*, 1996; *Schurgers et al.*, 2007]. Conversely, reforestation and surface darkening over boreal regions might amplify global warming [*Bonan et al.*, 1992; *Betts*, 2000]. Similarly, the North African humid period during the mid-Holocene likely required a substantial surface albedo reduction in the Sahara [*Laval and Picon*, 1986; *Kutzbach et al.*, 1996; *de Noblet-Ducoudré et al.*, 2000; *Bonfils et al.*, 2001; *Vamborg et al.*, 2011] and perhaps also in boreal regions [*Foley et al.*, 1994]. These albedo changes require changes in vegetation cover [*Xue and Shukla*, 1993; *Claussen and Gayler*, 1997], soil organic matter content [*Knorr and Schnitzler*, 2006], or soil moisture content [*Levis et al.*, 2004].

Despite the known importance of surface albedo, its representation in comprehensive global climate models and its influence on simulated climate remain poorly characterized. Some outstanding issues have been recognized: for instance, large intermodel albedo variability is found in boreal regions during winter and spring due to variability in snow and vegetation cover [*Lorant et al.*, 2014; *Wang et al.*, 2016; *Li et al.*, 2016]. The representation of tropical surface albedo variability in dry zones has been found to affect simulations of regional climate [*Sud and Fennessy*, 1982], especially in North Africa and the Middle East [*Knorr et al.*, 2001; *Samson et al.*, 2016]. Vegetation changes over boreal regions in climate models have also been found to alter simulated Intertropical Convergence Zone (ITCZ) and monsoons of West Africa and India [e.g., *McCarthy et al.*, 2012; *Swann et al.*, 2014]. Yet a global assessment of surface albedo bias in climate models and an understanding of the influence of this bias on simulated regional climate are lacking. Such an assessment may be particularly important during boreal summer in regions where thermal maxima lie over land [*Nie et al.*, 2010] and thus are highly sensitive to land surface properties. Here we document surface albedo bias and intermodel variability in the Coupled Model Intercomparison Project Phase 5 (CMIP5) then present results consistent with the hypothesis that intermodel variations in boreal summer albedo cause intermodel variations in regional precipitation. We also discuss previous results showing that model bias in land surface albedo can be caused by the prescription of land surface properties.

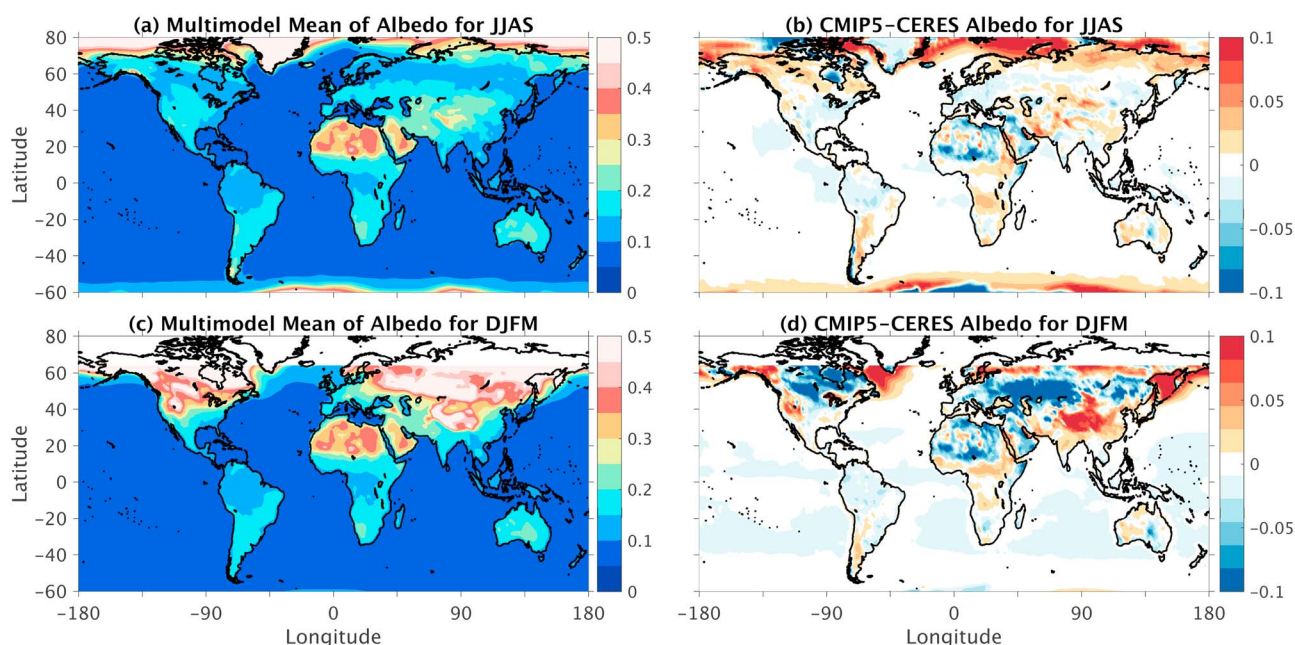


**Figure 1.** (a) CMIP5 ensemble mean of surface broadband shortwave albedo (abbreviated as albedo) for boreal summer (JJAS) averaged over last two decades of the historical run (1985 to 2004). (b) Ensemble mean JJAS albedo anomalies in CMIP5 with respect to the CERES observational data set; CERES albedo is averaged over the 2001 to 2015 period. (c) Same as Figure 1a but for boreal winter (DJFM). (d) Same as Figure 1b but for DJFM.

## 2. Data

Surface albedo and precipitation are compared across simulations from 47 CMIP5 models [Taylor *et al.*, 2012] listed in Supporting Information Table S1. All simulations are single-member hindcasts of the historical period (1850–2005; historical r1i1p1); here we only use data between 1985 and 2004 to allow comparison with satellite-derived observational products. We use monthly mean precipitation together with both upwelling and downwelling surface broadband shortwave radiative flux. We define a monthly mean surface broadband shortwave albedo (hereafter referred to as “albedo”) as the ratio of monthly mean surface upwelling to monthly mean surface downwelling shortwave radiative flux. Monthly means are combined into seasonal means, e.g., June–September (JJAS) for boreal summer and December–March (DJFM) for boreal winter. Albedo is regridded on a  $1^\circ \times 1^\circ$  grid using bilinear interpolation. The spatial resolution of CMIP5 output is coarser than the interpolated grid for all models except two (CMCC-CM and MIROC-4h; see Table S1), ensuring global conservation during interpolation [Kosaka *et al.*, 2009].

Model albedo is compared to that estimated from the Energy Balanced and Filled (EBAF) output of the Clouds and the Earth’s Radiant Energy System (CERES) mission. CERES EBAF-Surface\_Ed2.8 (hereafter CERES) provides monthly mean broadband shortwave and longwave fluxes at the surface on a  $1^\circ \times 1^\circ$  grid from March 2000 to February 2016, derived from daily top-of-atmosphere shortwave and longwave radiances on  $30 \text{ km} \times 30 \text{ km}$  horizontal footprints (see supporting information for details). Because of possible bias in the radiative transfer algorithm and inputs, CERES albedo is compared to Moderate Resolution Imaging Spectroradiometer (MODIS) and two other estimates obtained from the Surface Radiation Budget product of the Global Energy and Water Exchanges Project (GEWEX-SRB). The MODIS and SRB products cover different time periods and use different algorithms and inputs to compute surface fluxes (a detailed description of MODIS and SRB is in the supporting information). The multiyear means and interannual standard deviations of boreal summer albedo derived from MODIS and a recent version of the SRB product (SRB-TERRA) are similar to those from CERES (e.g., compare Figures 1b and 2d with supporting information Figures S1a, S1b, and S1c). On the other hand, comparison of CERES with an older version of SRB derived from the Earth Radiation Budget Experiment (SRB-ERBE) yields greater differences in boreal summer albedo (see Figure S1d in the supporting information). The better quality of radiance data and algorithms in CERES compared to SRB-ERBE and its strong agreement with MODIS motivate our use of CERES as the reference albedo product. While there is little temporal overlap between CERES (2000–2016) and the CMIP5 historical simulations (1985–2004), this does not likely alter our bias calculations because interannual variability in snow-free surface albedo is small in recent decades [e.g., Gupta *et al.*, 2001].

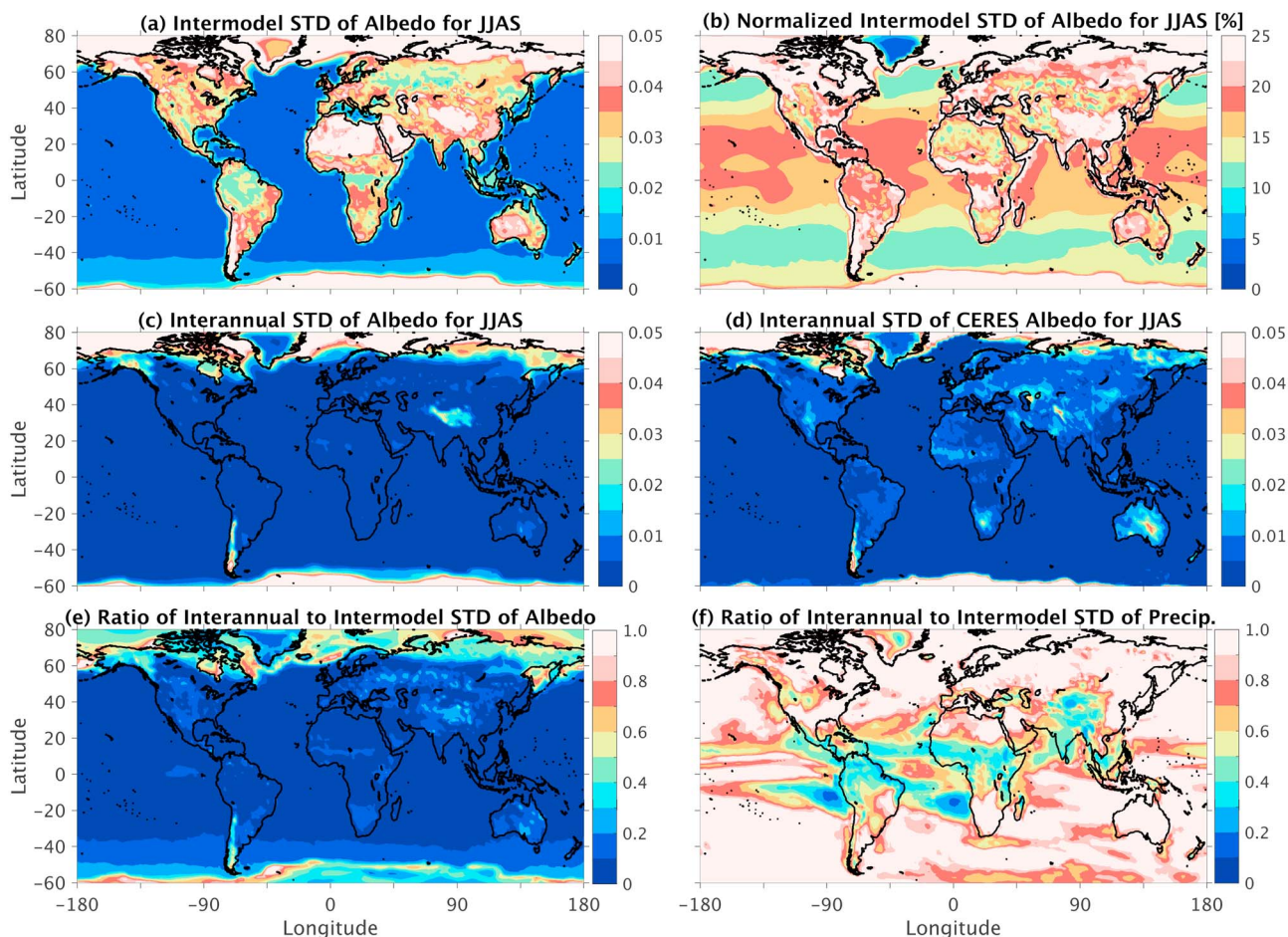


**Figure 2.** (a) Intermodel standard deviation of JJAS albedo in CMIP5 simulations. (b) Normalized intermodel standard deviation of JJAS albedo in CMIP5 simulations. (c) Interannual standard deviation of JJAS albedo in CMIP5 simulations. (d) Interannual standard deviation of JJAS albedo in CERES. (e) Ratio of interannual to intermodel standard deviation of JJAS albedo in CMIP5. (f) Same as in Figure 2e but for precipitation.

### 3. Results

#### 3.1. CMIP5 Bias and Intermodel Scatter

A well-known aspect of surface albedo is its large spatial variability: during boreal summer the CMIP5 multimodel mean albedo shows intense contrast between dark tropical rainforests, where albedo can be as low as 0.1, and bright subtropical and polar deserts, where albedo often exceeds 0.4 (Figure 1a). Although this spatial pattern is broadly consistent with observations, the multimodel mean albedo shows substantial bias over land when compared with CERES (Figure 1b). In some regions the magnitude of the albedo bias exceeds 0.1, which implies a bias in absorbed surface shortwave radiation on the order of tens of  $\text{W m}^{-2}$  (comparison with MODIS surface albedo yields a highly similar bias, supporting information Figure S1). During boreal summer, a large negative bias exists over the Saharan and Arabian deserts; smaller negative bias is also found over large swathes of the eastern U.S., the Amazon basin, and Europe (Figure 1b). Positive bias exists over nearly all other land regions. Oceans show comparatively weak but nonzero bias.

During boreal winter, snow cover causes large surface brightening in the northern extratropics and over the Tibetan Plateau (Figure 1c), which are regions of large bias in the multimodel mean (Figure 1d). While snow cover bias in models has been shown to be large and to influence simulated global climate [e.g., *Randall et al., 1994; Qu and Hall, 2006*], we henceforth focus on the less well-known biases found during boreal summer. Although smaller in magnitude than the wintertime snow-related albedo bias, the albedo bias over low-latitude land will influence the land surface enthalpy fluxes that control the time-mean overturning circulations that organize tropical precipitation [e.g., *Charney, 1975; Xue and Shukla, 1993*].

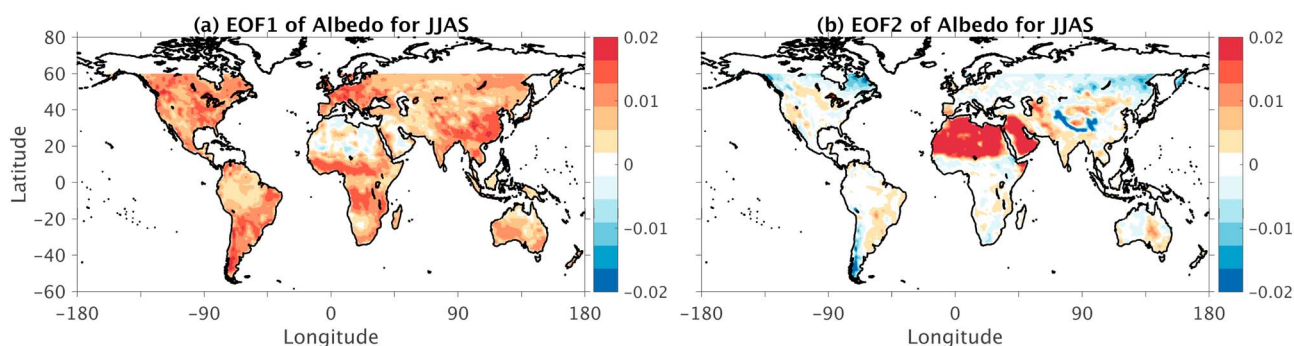


**Figure 3.** (a) First EOF of the intermodel variability of albedo in CMIP5 simulations for JJAS (1984–2004); (b) same as Figure 3a but for the second EOF. EOF1 explains about 35% of global variance, and EOF2 17%.

The intermodel spread of boreal summer albedo is similar in magnitude to the multimodel mean seasonal bias in many locations (compare Figures 1b and 2a). To first-order, intermodel variability increases with albedo, being largest over polar regions, subtropical deserts, and highlands, and smallest over forests and oceans. Intermodel standard deviation of albedo varies between 10 and 25% of its multimodel mean value over most regions (Figure 2b); relative to its local value, intermodel albedo variability over snow-free regions is large over tropical vegetated regions and midlatitudes, and lowest over deserts. Intermodel variability is particularly strong over boreal monsoon regions (i.e., West Africa, India, and China), and over land areas north of 45°N (Figure 2b). Relative intermodel albedo variability is substantial over oceans, where the intermodel standard deviation varies between 15% and 20% of the multimodel mean in the tropics.

Intermodel variance of boreal summer albedo is much larger than the multimodel mean of the interannual variance of that albedo (Figures 2a, 2c, and 2e). The latter is negligible nearly everywhere except over elevated terrain and polar regions where variations in snow and ice cover can cause large albedo variability. The small interannual variability of albedo in CMIP5 simulations is broadly consistent with the small interannual variability of observed albedo (Figure 2d). In contrast, interannual variability in precipitation is comparable to intermodel variability in precipitation (Figure 2f). This is one piece of evidence supporting the hypothesis that albedo bias in individual models is not caused by precipitation bias. Specifically, if a precipitation variation  $\delta P$  caused a local surface albedo variation  $\delta\alpha$ , we would expect to be able to write the latter as a function of the former. Since the historical CMIP5 simulations do not employ dynamic vegetation [see Taylor *et al.*, 2009, Table 3], this function will not depend on the time scale of the variation as long as that time scale is seasonal or longer (i.e., the time needed for adjustment of soil moisture or leaf area). So unless the function relating  $\delta\alpha$  to  $\delta P$  is strongly nonlinear,

$$\frac{\delta\alpha_{\text{interannual}}}{\delta\alpha_{\text{intermodel}}} \approx \frac{\delta P_{\text{interannual}}}{\delta P_{\text{intermodel}}}, \quad (1)$$

where the subscript denotes the type of variation. Since the left-hand side of (1) is much smaller than the right-hand side in CMIP5 (Figures 2e and 2f), this implies that model precipitation bias does not cause local model albedo bias.

To reveal spatial patterns of intermodel albedo variability, we perform a principal component analysis on boreal summer albedo. We restrict the domain of analysis to land within 60°S–60°N to exclude polar snow-covered regions. The first and second modes of variability, PC1 and PC2, explain 35% and 17% of intermodel variance, respectively, while higher modes explain less than 7% each. Maps of the empirical orthogonal functions (EOFs) corresponding to the first two modes highlight geographically distinct patterns. EOF1 represents albedo variation over most land regions excluding the Sahara and Middle East (Figure 3a), while EOF2 primarily represents variations over the Saharan and Arabian deserts (Figure 3b). Broadly, the first and second modes represent regions with and without vegetation cover, respectively. We henceforth focus mostly on EOF1 since it accounts for a larger fraction of intermodel albedo variance but recognize that albedo bias over the Sahara may be of great importance for Sahel rainfall [e.g., Charney, 1975].

### 3.2. Precipitation-Albedo Association

The large intermodel variability of albedo and its coherence on planetary scales may have consequences for simulated low-latitude precipitation, given that surface albedo is known to influence precipitating tropical

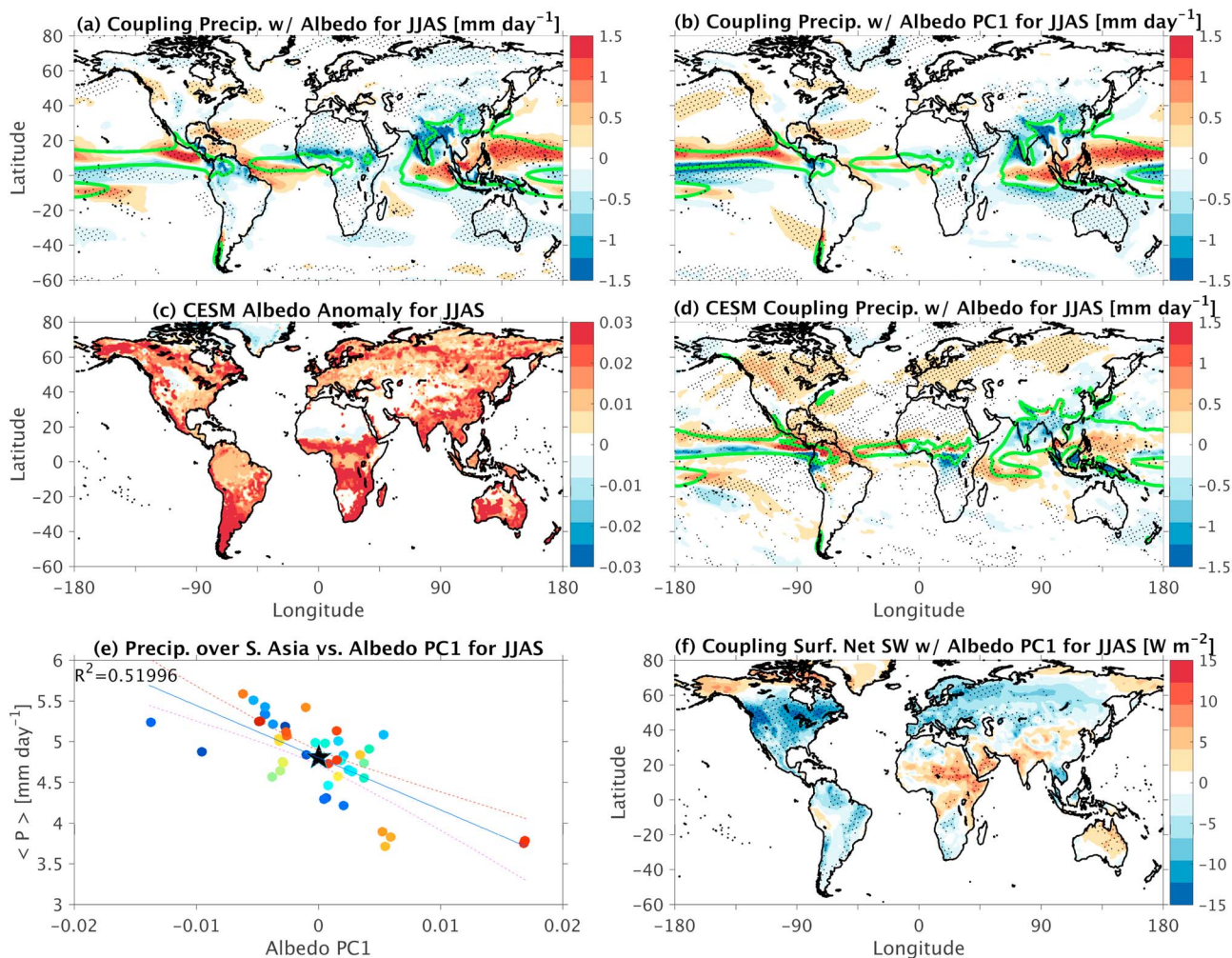


**Figure 4.** Coupling of CMIP5 precipitation ( $\text{mm day}^{-1}$ ) with (a) local albedo and (b) albedo PC1. (c) Prescribed CSM albedo anomaly and (d) coupling of CSM precipitation ( $\text{mm day}^{-1}$ ) with that anomaly. (e) Relation of CMIP5 South Asian precipitation (land only,  $60^\circ - 180^\circ\text{E}$ ,  $5^\circ - 45^\circ\text{N}$ ) with albedo PC1; blue line shows the best linear fit and dashed lines the 95% confidence interval on the regression line. (f) Coupling of CMIP5 net surface shortwave flux ( $\text{W m}^{-2}$ ) with albedo PC1. Areas statistically significant at 5% level are stippled in Figures 4a, 4b, 4d, and 4f. Significance in CSM is found where changes in precipitation between the control and perturbation have the same sign in at least 95% of 1000 bootstrap samples.

circulations [e.g., Charney, 1975; Eltahir, 1996; Zeng and Neelin, 1999]. To gauge the association between albedo  $\alpha$  and precipitation  $P$ , we define a coupling index

$$I(P, \alpha) = \sigma(\alpha) \frac{\partial P}{\partial \alpha}, \quad (2)$$

where  $\sigma(\alpha)$  is the intermodel standard deviation of  $\alpha$  and  $\partial_\alpha P$  is obtained from linear regression of  $P$  on  $\alpha$ . A similar measure was used to assess the association of soil moisture with precipitation [Dirmeyer, 2011], and  $I$  simply scales the regression coefficient by the intermodel variability in  $\alpha$ .

When the local values of boreal summer  $P$  and  $\alpha$  are used to compute  $I$  at every location, the strongest local association between continental precipitation and albedo is found over India, the Sahel, and eastern China (Figure 4a). Over land, precipitation is almost always anticorrelated with albedo, consistent with the idea of brighter surfaces disfavoring local continental precipitation [e.g., Charney, 1975] or with the idea of wet land having a lower albedo (e.g., due to the darker color of wet soil). But given the strong spatial correlations in intermodel albedo variations (e.g., Figure 3a), a strong local correlation between variations in precipitation and albedo does not necessarily imply local causation. Indeed, it would be surprising if local ocean albedo variations in the West Pacific caused the increase in equatorial central Pacific rainfall seen in Figure 4a, given the small magnitude of ocean albedo variations (e.g., Figure 2a). So we compare this distribution of  $I$ , which was

computed from local values of  $\alpha$  and  $P$ , to another version computed using the intermodel albedo anomaly that projects on EOF1,  $I(P, \langle \alpha_1 \rangle)$ . Here  $\langle \cdot \rangle$  is an area-weighted average over all land regions within  $60^\circ\text{S}$  to  $60^\circ\text{N}$ , and  $\alpha_1$  is the intermodel albedo anomaly that projects on the first EOF, i.e.,  $\alpha_1 = \text{PC1}(\alpha) \times \text{EOF1}(\alpha)$ . The association of  $P$  with  $\langle \alpha_1 \rangle$  is similar to the local association: e.g., strong association exists over large parts of South and East Asia (Figure 4b). The tropical Pacific association now clearly represents a northward shift in the ITCZ over much of the Pacific in models having high albedo of vegetated land. Also,  $I(P, \langle \alpha_1 \rangle)$  is weaker than the local coupling index  $I(P, \alpha)$  over central India and the Sahel; this difference likely arises from a combination of precipitation variations projecting more strongly onto EOF2 albedo (supporting information Figure S2d), or precipitation-albedo covariability being mediated locally by soil moisture (supporting information Figure S4d). Similar results are obtained when the association of  $P$  and  $\alpha$  is assessed using a maximum covariance analysis, as shown in supporting information Figure S2.

These associations are generally consistent with the hypothesis that brighter land surfaces cause a reduction in continental precipitation. Intermodel albedo variability is associated with variability in the shortwave radiative flux absorbed at the surface (Figure 4f). In particular, an increase of global albedo over vegetated regions by one standard deviation of its intermodel spread,  $\sigma(\langle \alpha_1 \rangle)$ , is accompanied by a reduction in absorbed surface shortwave of  $5\text{--}10\text{ W m}^{-2}$  over extensive areas of North America and Eurasia (Figure 4f). This is consistent with the hypothesis that extratropical northern land influences tropical precipitation [McCarthy *et al.*, 2012; Swann *et al.*, 2014]: an increase in albedo over that land reduces the net surface shortwave absorbed and the surface enthalpy fluxes into the overlying atmosphere, causing a southward shift of precipitation over tropical land in the Northern Hemisphere (e.g., note precipitation shifts from India to the Maritime continent as global albedo brightens in Figure 4b). Despite large regional shifts in precipitation, no meridional shift in precipitation is found in the zonal mean, due to a large cancelation in the meridional shift of regional ITCZs (not shown). This suggests either that vegetated land albedo does not strongly influence the zonal-mean column-integrated atmospheric energy budget [Chiang and Bitz, 2005; Broccoli *et al.*, 2006; Kang *et al.*, 2008; Chiang and Friedman, 2012; Donohoe *et al.*, 2013] or that there are compensating changes in the zonal-mean gross moist stability or in zonal-mean feedbacks (e.g., due to clouds). This contrasts with the precipitation shifts shown to be caused directly by surface albedo changes in cloud-free regions such as the Sahara [e.g., Charney, 1975; Boos and Korty, 2016].

Regardless of the cause of the albedo-precipitation relationship, the fraction of intermodel precipitation variance associated with intermodel albedo variations is large in many regions. In particular, South Asia, the southern Indian Ocean, Australia, and the East Pacific ITCZ region all have large regression coefficients (Figures 4a and 4b). The square of the correlation coefficient nears or reaches 0.5 in individual grid cells in those regions (Figure S3). When precipitation is averaged over continental South Asia ( $60^\circ\text{--}180^\circ\text{E}$ ,  $5^\circ\text{--}45^\circ\text{N}$ ; land only) and regressed on PC1 of albedo (Figure 4e), nearly half of the intermodel variance in South Asian boreal summer precipitation is found to project on global (PC1) intermodel variations of albedo. Such a strong association is not found when comparing intermodel precipitation variance with intermodel variability of other surface variables such as soil moisture (supporting information Figure S4).

### 3.3. Precipitation Sensitivity to Albedo in CESM

Our regression analysis cannot separate the local and remote associations between albedo and precipitation due to the planetary-scale coherence of intermodel albedo variability, nor it can definitively establish causation between albedo and precipitation variations. To address this problem, we simulate the precipitation response to a global albedo anomaly imposed in vegetated regions.

We use the Community Earth System Model (CESM) version 1.0.4 from the National Center for Atmospheric Research. This model consists of a global atmospheric model (the Community Atmosphere Model, version 5) coupled to a dynamical ocean (the Parallel Ocean Program, version 2), sea ice (CICE4), land ice (GLC), and a comprehensive land model (CLM). In a control simulation, we integrate CESM with Earth's present-day radiative forcings and boundary conditions (B2000 configuration), with horizontal resolution of  $0.9^\circ \times 1.25^\circ$  and 26 vertical levels for the atmosphere, and a nominal ocean resolution of  $1^\circ$ . This control is run for 100 years with output averaged over the last 80 years. In a perturbation simulation we run CESM with modified land albedo: over regions where the direct beam albedo is lower than 0.15, both direct and diffuse albedos are set to 0.01. This modifies the CESM broadband surface albedo, which we refer to as  $\alpha_{\text{CESM}}$ , to be darker in vegetated regions in a spatial pattern broadly resembling albedo EOF1 (compare Figures 3a and 4c).

To compare the precipitation response to this CESM albedo anomaly with the association between intermodel precipitation and albedo variations in CMIP5, we define a coupling index

$$I(P, \langle \alpha_{\text{CESM}} \rangle) = \sigma(\langle \alpha_1 \rangle) \frac{\Delta P}{\Delta \langle \alpha_{\text{CESM}} \rangle}, \quad (3)$$

where  $\Delta$  signifies a difference between the control and perturbation CESM integrations. To facilitate comparison with the CMIP5 results, we construct (3) by scaling the CESM sensitivity by the intermodel standard deviation of albedo EOF1 obtained from the CMIP5 models,  $\sigma(\langle \alpha_1 \rangle)$ . This coupling index has many similarities to the coupling index between precipitation and albedo EOF1 in the CMIP5 simulations,  $I(P, \langle \alpha_1 \rangle)$ , as seen in Figures 4d and 4b. In particular, brighter albedo over vegetated regions decreases precipitation over South Asia and Australia but increases rainfall over the equatorial East Indian Ocean; similarity is particularly strong over the East Pacific, where the ITCZ shifts poleward as land albedo brightens, and it is remarkable that the CESM response has a magnitude that is overall similar to that of the albedo-related intermodel precipitation variations seen in CMIP5. Substantial differences also exist between the CMIP5 associations and the CESM response, particularly in the Sahel, Central Africa, North America, and Northern Eurasia. Yet the CESM result broadly supports our hypothesis that intermodel differences in land albedo cause nonlocal intermodel precipitation variations in CMIP5.

#### 4. Discussion: Causes of Albedo Bias

Understanding the cause of albedo bias and intermodel albedo variability is challenging due to both model complexity and lack of detailed output about the radiative properties of the surface and atmosphere. Nevertheless, the near-global coherence of intermodel albedo variations over continental regions and their weak interannual variability suggest that model albedo variations are unlikely to be driven by a quantity with large spatial or interannual variability, such as precipitation. Instead, a spatially homogeneous quantity might cause spatially coherent albedo variability, for instance by modifying atmospheric radiative properties. For example, tropospheric water vapor, which has higher homogeneity across the tropics than precipitation, preferentially absorbs shortwave in the near-infrared (IR) [Pierrehumbert, 2010]; since vegetated surfaces have lower albedo in the visible than in the near-IR [Houldcroft *et al.*, 2009], greater tropospheric water vapor could reduce broadband surface albedo. Another potential source of albedo variability is the illumination angle [Song, 1998], particularly the relative contribution of diffuse and direct shortwave flux reaching the surface, because white-sky (i.e., diffuse) albedo is typically 10% to 15% larger than black sky (i.e., direct local noon) albedo (see MODIS estimates in Houldcroft *et al.* [2009]). Water vapor and other species (e.g., aerosols) can thus bias broadband surface albedo by absorption or scattering. Clouds can amplify these biases, with reflection between surface and clouds substantially increasing the path length over which extinction occurs [Ambach, 1974].

We obtained a rough estimate of the influence of these processes on broadband shortwave albedo through idealized calculations conducted with the Fu-Liou radiative transfer code [Fu and Liou, 1993]. Using typical land surfaces (e.g., mixed forest, woody savannah, and grassland) as a lower boundary and typical tropical conditions (e.g., temperature and atmospheric constituents), we estimated changes in broadband shortwave albedo in a cloud-free atmosphere due to changing tropospheric water vapor and solar zenith angle. Land surface albedo typically increased by 5%–20% of its original value when water vapor was reduced from its tropical-mean value to near zero, while it increased by up to 20% when solar radiation was changed from direct beam at noon to isotropic, diffuse illumination. Since the CMIP5 intermodel variations in tropical-mean specific humidity and illumination angle are expected to be much smaller than these limiting cases, it seems unlikely that these factors could cause the large intermodel albedo variations found here (the intermodel standard deviation exceeds 20% over many land regions, e.g., Figure 2b). On the other hand, intermodel variations in shortwave absorption or scattering might be important in regions where albedo has a lower intermodel variability relative to its mean (e.g., deserts).

Another hypothesis is that intermodel albedo variability is caused by different prescriptions of soil and vegetation properties among models. Models use different distributions of plant functional types (PFTs) when representing identical land use. This is true for all land types, from the most to the least affected by human activity (e.g., cropland versus primary forest) [de Noblet-Ducoudré *et al.*, 2012]. Bias in PFT distributions has been shown to produce surface albedo bias of up to 25% [e.g., Matthes *et al.*, 2016]. The spatial coherence

in albedo variability could result from the relatively small number of PFTs used in land models, typically less than 15 [Brovkin *et al.*, 2013a]. Biomes covering extensive areas such as broadleaf deciduous forests or grasslands are represented by only a handful of PFTs (typically less than 4) sharing similar properties (for specific examples of PFT implementation in land models, see Brovkin *et al.* [2013b], Houldcroft *et al.* [2009], Bonan *et al.* [2002], and Krinner *et al.* [2005]). Land models also differ in their representations of PFT interactions with radiation; for instance, differences in canopy shortwave flux absorption could bias surface albedo even if soil albedo and PFTs are unbiased [e.g., Betts, 2000].

Differences in soil moisture and organic matter also lead to albedo bias if organic matter or soil moisture is either set dynamically or not consistently prescribed among models [e.g., Levis *et al.*, 2004; Vamborg *et al.*, 2011]. While intermodel variations in boreal summer albedo are correlated with intermodel variations in soil moisture in certain regions, such as the Sahel and India, no significant relationship between these variations is found on planetary scales, suggesting that soil moisture is not the primary driver of intermodel albedo variability during boreal summer (supporting information Figure S4). In summary, model representations of albedo can be influenced by the simulated climatological mean state and its influence on shortwave scattering and absorption, yet previous studies [e.g., Matthes *et al.*, 2016] and our aforementioned idealized radiative transfer calculation indicate that albedo bias in individual models is more likely caused by bias in surface properties such as PFTs or in canopy radiative transfer.

## 5. Conclusions

The intermodel variations of surface albedo found here are spatially coherent over all vegetated land and are distinct from variations over desert and snow-covered regions that have been found to influence simulated climate [e.g., Wang *et al.*, 2016; Samson *et al.*, 2016]. This dominant mode of intermodel albedo variability correlates with intermodel variability in low-latitude precipitation, with brighter vegetated surfaces associated with a southward shift of precipitation from South Asia toward the equatorial Indian Ocean and a northward shift of the East Pacific ITCZ.

We have not definitively established the cause of this albedo-precipitation association but presented several pieces of evidence consistent with the hypothesis that intermodel albedo variations cause intermodel precipitation variations. First, the large difference in the spatial structures of intermodel variations of precipitation and albedo suggests that the interaction is not local. This, together with the weak relationship between the dominant modes of intermodel variability of albedo and soil moisture (supporting information Figure S4), and intermodel albedo variations being much larger than simulated interannual albedo variations, suggests that the intermodel albedo variance is not simply caused by intermodel variations in precipitation or surface water (e.g., wetter soils being darker). Furthermore, previous work [Matthes *et al.*, 2016] showed that model differences in vegetation distribution can produce surface albedo bias of up to 25%. Finally, we showed that in one global climate model, prescribing an albedo anomaly similar to the dominant mode of intermodel albedo variability caused precipitation shifts similar to those of the intermodel albedo-precipitation association. The dynamics governing this response are unclear, even in a single model, but may involve zonally asymmetric precipitation perturbations caused by extratropical land albedo. Future work is needed to determine whether energy budget theories for ITCZ location [e.g., Kang *et al.*, 2008; Donohoe *et al.*, 2013; Boos and Korty, 2016] can explain these associations between albedo and precipitation anomalies.

Intermodel variability in tropical precipitation has previously been attributed to diversity in model representations of various other processes and surface conditions, e.g., SST [e.g., Li and Xie, 2012, 2014], moist convective physics [e.g., Hirota and Takayabu, 2013; Tomassini *et al.*, 2015], cloud cover [e.g., Hwang and Frierson, 2013; Li and Xie, 2014], snow cover and soil moisture [e.g., Yasunari *et al.*, 1991; Xu and Dirmeyer, 2013], topography [e.g., Boos and Hurley, 2013], and aerosols [e.g., Guo *et al.*, 2015]. The planetary-scale intermodel variability in surface albedo demonstrated here may be an additional large source of intermodel precipitation variance, especially over the Asian monsoon region. We argued that differing representations of vegetation and soil properties are a likely cause of these albedo variations, with variations in mean climate variables such as water vapor, soil moisture, aerosols, and clouds playing a lesser role. The lack of spectrally resolved radiative flux output in CMIP5 unfortunately prevents quantification of these effects. Although further work is needed to determine whether remediating albedo bias will reduce precipitation bias, this seems a promising approach for addressing longstanding biases in tropical rainfall, such as the dry bias that has persisted over continental India through generations of climate models [e.g., Sperber *et al.*, 2013].

## Acknowledgments

We acknowledge support from Office of Naval Research award N00014-15-1-2531 and National Science Foundation awards AGS-1253222 and AGS-1515960. CMIP5 output were obtained from the World Data Center for Climate (WDCC) website at <https://cera-www.dkrz.de>. The CERES EBAF-Surface\_Ed2.8 product is available from the National Aeronautics and Space Administration (NASA) at <https://ceres.larc.nasa.gov/>. The MODIS Gap-Filled Product (MCD43GF) is available from Crystal SchAAF's website at the University of Massachusetts, Boston, [https://www.umb.edu/spectralmass/terra\\_aqua\\_modis/v006/](https://www.umb.edu/spectralmass/terra_aqua_modis/v006/). GEWEX-SRB products are available from NASA at <https://gewex-srb.larc.nasa.gov/>. The Fu-Liou radiative transfer code is available at <https://www.cave.larc.nasa.gov/cgi-bin/fuliou/runfi.cgi> as part of the CERES/ARM Validation Experiment. X. Levine thanks Ravi Shekhar for many helpful discussions. This manuscript greatly benefited from comments by two anonymous reviewers.

## References

- Ambach, W. (1974), The influence of cloudiness on the net radiation balance of a snow surface with high albedo, *J. Glaciol.*, *13*(67), 73–84.
- Betts, R. A. (2000), Offset of the potential carbon sink from boreal forestation by decreases in surface albedo, *Nature*, *408*(6809), 187–190.
- Bonan, G. B., D. Pollard, and S. L. Thompson (1992), Effects of boreal forest vegetation on global climate, *Nature*, *359*, 716–718.
- Bonan, G. B., S. Levis, L. Kergoat, and K. W. Oleson (2002), Landscapes as patches of plant functional types: An integrating concept for climate and ecosystem models, *Global Biogeochem. Cycles*, *16*(2), 1021, doi:10.1029/2000GB001360.
- Bonfils, C., N. de Noblet-Ducoudré, P. Braconnot, and S. Joussaume (2001), Hot desert albedo and climate change: Mid-Holocene monsoon in North Africa, *J. Clim.*, *14*(17), 3724–3737.
- Boos, W. R., and J. V. Hurlley (2013), Thermodynamic bias in the multimodel mean boreal summer monsoon, *J. Clim.*, *26*(7), 2279–2287.
- Boos, W. R., and R. L. Korty (2016), Regional energy budget control of the intertropical convergence zone and application to mid-Holocene rainfall, *Nat. Geosci.*, *9*(12), 892–897.
- Brocchi, A. J., K. A. Dahl, and R. J. Stouffer (2006), Response of the ITCZ to Northern Hemisphere cooling, *Geophys. Res. Lett.*, *33*, L01702, doi:10.1029/2005GL024546.
- Brovkin, V., et al. (2013a), Effect of anthropogenic land-use and land-cover changes on climate and land carbon storage in CMIP5 projections for the twenty-first century, *J. Clim.*, *26*(18), 6859–6881.
- Brovkin, V., L. Boysen, T. Raddatz, V. Gayler, A. Loew, and M. Claussen (2013b), Evaluation of vegetation cover and land-surface albedo in MPI-ESM CMIP5 simulations, *J. Adv. Model. Earth Syst.*, *5*, 48–57, doi:10.1029/2012MS000169.
- Charney, J. G. (1975), Dynamics of deserts and drought in the Sahel, *Q. J. R. Meteorol. Soc.*, *101*(428), 193–202.
- Chiang, J. C. H., and C. M. Bitz (2005), Influence of high latitude ice cover on the marine Intertropical Convergence Zone, *Clim. Dyn.*, *25*(5), 477–496.
- Chiang, J. C. H., and A. R. Friedman (2012), Extratropical cooling, interhemispheric thermal gradients, and tropical climate change, *Annu. Rev. Earth Planet. Sci.*, *40*, 383–412.
- Claussen, M., and V. Gayler (1997), The greening of the Sahara during the mid-Holocene: Results of an interactive atmosphere-biome model, *Global Ecol. Biogeogr. Lett.*, *6*, 369–377.
- de Noblet, N. I., I. C. Prentice, S. Joussaume, D. Texier, A. Botta, and A. Haxeltine (1996), Possible role of atmosphere-biosphere interactions in triggering the Last Glaciation, *Geophys. Res. Lett.*, *23*(22), 3191–3194.
- de Noblet-Ducoudré, N., M. Claussen, and I. C. Prentice (2000), Mid-Holocene greening of the Sahara: First results of the GAIM 6000 year BP experiment with two asynchronously coupled atmosphere/biome models, *Clim. Dyn.*, *16*(9), 643–659.
- de Noblet-Ducoudré, N., et al. (2012), Determining robust impacts of land-use-induced land cover changes on surface climate over North America and Eurasia: Results from the first set of LUCID experiments, *J. Clim.*, *25*(9), 3261–3281.
- Dirmeyer, P. A. (2011), The terrestrial segment of soil moisture-climate coupling, *Geophys. Res. Lett.*, *38*, L16702, doi:10.1029/2011GL048268.
- Donohoe, A., J. Marshall, D. Ferreira, and D. Mcgee (2013), The relationship between ITCZ location and cross-equatorial atmospheric heat transport: From the seasonal cycle to the Last Glacial Maximum, *J. Clim.*, *26*(11), 3597–3618.
- Eltahir, E. A. B. (1996), Role of vegetation in sustaining large-scale atmospheric circulations in the tropics, *J. Geophys. Res.*, *101*(D2), 4255–4268.
- Foley, J. A., J. E. Kutzbach, M. T. Coe, and S. Levis (1994), Feedbacks between climate and boreal forests during the Holocene epoch, *Nature*, *371*, 52–54.
- Fu, Q., and K. N. Liou (1993), Parameterization of the radiative properties of cirrus clouds, *J. Atmos. Sci.*, *50*(13), 2008–2025.
- Guo, L., A. G. Turner, and E. J. Highwood (2015), Impacts of 20th century aerosol emissions on the South Asian monsoon in the CMIP5 models, *Atmos. Chem. Phys.*, *15*(11), 6367–6378.
- Gupta, S. K., D. P. Kratz, P. W. Stackhouse Jr., and A. C. Wilber (2001), *The Langley Parameterized Shortwave Algorithm (LPSA) for Surface Radiation Budget Studies*, NASA, Hampton, Va.
- Hirota, N., and Y. N. Takayabu (2013), Reproducibility of precipitation distribution over the tropical oceans in CMIP5 multi-climate models compared to CMIP3, *Clim. Dyn.*, *41*(11–12), 2909–2920.
- Houldcroft, C. J., W. M. F. Grey, M. Barnsley, C. M. Taylor, S. O. Los, and P. R. J. North (2009), New vegetation albedo parameters and global fields of soil background albedo derived from MODIS for use in a climate model, *J. Hydrometeorol.*, *10*(1), 183–198.
- Hwang, Y.-T., and D. M. Frierson (2013), Link between the double-intertropical convergence zone problem and cloud biases over the Southern Ocean, *Proc. Natl. Acad. Sci. U.S.A.*, *110*(13), 4935–4940.
- Kang, S. M., I. M. Held, D. M. Frierson, and M. Zhao (2008), The response of the ITCZ to extratropical thermal forcing: Idealized slab-ocean experiments with a GCM, *J. Clim.*, *21*(14), 3521–3532.
- Knorr, W., and K.-G. Schnitzler (2006), Enhanced albedo feedback in North Africa from possible combined vegetation and soil-formation processes, *Clim. Dyn.*, *26*(1), 55–63.
- Knorr, W., K.-G. Schnitzler, and Y. Govaerts (2001), The role of bright desert regions in shaping North African climate, *Geophys. Res. Lett.*, *28*(18), 3489–3492.
- Kosaka, Y., H. Nakamura, M. Watanabe, and M. Kimoto (2009), Analysis on the dynamics of a wave-like teleconnection pattern along the summertime Asian jet based on a reanalysis dataset and climate model simulations, *J. Meteorol. Soc. Jpn. Ser. II*, *87*(3), 561–580.
- Krinner, G., N. Viovy, N. de Noblet-Ducoudré, J. Ogée, J. Polcher, P. Friedlingstein, P. Ciais, S. Sitch, and I. C. Prentice (2005), A dynamic global vegetation model for studies of the coupled atmosphere-biosphere system, *Global Biogeochem. Cycles*, *19*, GB1015, doi:10.1029/2003GB002199.
- Kutzbach, J., G. Bonan, J. Foley, and S. P. Harrison (1996), Vegetation and soil feedbacks on the response of the African monsoon to orbital forcing in the early to middle Holocene, *Nature*, *384*(6610), 623–626.
- Laval, K., and L. Picon (1986), Effect of a change of the surface albedo of the Sahel on climate, *J. Atmos. Sci.*, *43*(21), 2418–2429.
- Levis, S., G. B. Bonan, and C. Bonfils (2004), Soil feedback drives the mid-Holocene North African monsoon northward in fully coupled CCSM2 simulations with a dynamic vegetation model, *Clim. Dyn.*, *23*(7–8), 791–802.
- Li, G., and S.-P. Xie (2012), Origins of tropical-wide SST biases in CMIP multi-model ensembles, *Geophys. Res. Lett.*, *39*, L22703, doi:10.1029/2012GL053777.
- Li, G., and S.-P. Xie (2014), Tropical biases in CMIP5 multimodel ensemble: The excessive equatorial Pacific cold tongue and double ITCZ problems, *J. Clim.*, *27*(4), 1765–1780.
- Li, Y., T. Wang, Z. Zeng, S. Peng, X. Lian, and S. Piao (2016), Evaluating biases in simulated land surface albedo from CMIP5 global climate models, *J. Geophys. Res. Atmos.*, *121*, 6178–6190, doi:10.1002/2016JD024774.
- Lorant, M. M., L. T. Berner, S. J. Goetz, Y. Jin, and J. T. Randerson (2014), Vegetation controls on northern high latitude snow-albedo feedback: Observations and CMIP5 model simulations, *Global Change Biol.*, *20*(2), 594–606.

- Matthes, J. H., S. Goring, J. W. Williams, and M. C. Dietze (2016), Benchmarking historical CMIP5 plant functional types across the Upper Midwest and Northeastern United States, *J. Geophys. Res. Biogeosci.*, *121*, 523–535.
- McCarthy, M. P., J. Sanjay, B. B. Booth, K. Krishna Kumar, and R. A. Betts (2012), The influence of vegetation on the ITCZ and South Asian monsoon in HadCM3, *Earth Syst. Dyn.*, *3*(1), 87–96.
- Nie, J., W. R. Boos, and Z. Kuang (2010), Observational evaluation of a convective quasi-equilibrium view of monsoons, *J. Clim.*, *23*(16), 4416–4428.
- Pierrehumbert, R. T. (2010), 5: Scattering, in *Principles of Planetary Climate*, edited by R. T. Pierrehumbert, pp. 316–385, Cambridge Univ. Press, Cambridge, U. K.
- Qu, X., and A. Hall (2006), Assessing snow albedo feedback in simulated climate change, *J. Clim.*, *19*(11), 2617–2630.
- Randall, D. A., et al. (1994), Analysis of snow feedbacks in 14 general circulation models, *J. Geophys. Res.*, *99*(D10), 20,757–20,771.
- Samson, G., S. Masson, F. Durand, P. Terray, S. Berthet, and S. Jullien (2016), Roles of land surface albedo and horizontal resolution on the Indian summer monsoon biases in a coupled ocean–atmosphere tropical-channel model, *Clim. Dyn.*, *48*, 1571–1594.
- Schurgers, G., U. Mikolajewicz, M. Gröger, E. Maier-Reimer, M. Vizcaino, and A. Winguth (2007), The effect of land surface changes on Eemian climate, *Clim. Dyn.*, *29*(4), 357–373.
- Song, J. (1998), Diurnal asymmetry in surface albedo, *Agric. For. Meteorol.*, *92*(3), 181–189.
- Sperber, K. R., H. Annamalai, I. S. Kang, A. Kitoh, A. Moise, A. Turner, B. Wang, and T. Zhou (2013), The Asian summer monsoon: An intercomparison of CMIP5 vs. CMIP3 simulations of the late 20th century, *Clim. Dyn.*, *41*(9–10), 2711–2744.
- Sud, Y. C., and M. Fennessy (1982), A study of the influence of surface albedo on July circulation in semi-arid regions using the GLAS GCM, *J. Climatol.*, *2*(2), 105–125.
- Swann, A. L. S., I. Y. Fung, Y. Liu, and J. C. H. Chiang (2014), Remote vegetation feedbacks and the mid-Holocene green Sahara, *J. Clim.*, *27*(13), 4857–4870.
- Taylor, K. E., R. J. Stouffer, and G. A. Meehl (2009), *A Summary of the CMIP5 Experiment Design*, 33 pp., Program For Clim. Model Diagnosis and Intercomparison, Livermore, Calif.
- Taylor, K. E., R. J. Stouffer, and G. A. Meehl (2012), An overview of CMIP5 and the experiment design, *Bull. Am. Meteorol. Soc.*, *93*(4), 485–498.
- Tomassini, L., A. Voigt, and B. Stevens (2015), On the connection between tropical circulation, convective mixing, and climate sensitivity, *Q. J. R. Meteorol. Soc.*, *141*(689), 1404–1416.
- Vamborg, F. S. E., V. Brovkin, and M. Claussen (2011), The effect of a dynamic background albedo scheme on Sahel/Sahara precipitation during the mid-Holocene, *Clim. Past*, *7*(1), 117–131.
- Wang, L., J. N. Cole, P. Bartlett, D. Versegny, C. Derksen, R. Brown, and K. Salzen (2016), Investigating the spread in surface albedo for snow-covered forests in CMIP5 models, *J. Geophys. Res. Atmos.*, *121*, 1104–1119, doi:10.1002/2015JD023824.
- Xu, L., and P. Dirmeyer (2013), Snow–atmosphere coupling strength. Part I: Effect of model biases, *J. Hydrometeorol.*, *14*(2), 389–403.
- Xue, Y., and J. Shukla (1993), The influence of land surface properties on Sahel climate. Part 1: desertification, *J. Clim.*, *6*(12), 2232–2245.
- Yasunari, T., A. Kitoh, and T. Tokioka (1991), Local and remote responses to excessive snow mass over Eurasia appearing in the northern spring and summer climate, *J. Meteorol. Soc. Jpn. Ser. II*, *69*(4), 473–487.
- Zeng, N., and J. D. Neelin (1999), A land-atmosphere interaction theory for the tropical deforestation problem, *J. Clim.*, *12*(3), 857–872.